A Genetically Encoded Thiophenol Recruits Noble Metals for Designer Enzymes

Mathijs J. Veen[1], Friso S. Aalbers[1], Henriëtte J. Rozeboom[2],

Andy-Mark W.H. Thunnissen[2], Daniel F. Sauer[1]* and Gerard Roelfes[1]*

[1] Stratingh Institute for Chemistry, University of Groningen, 9747 AG, Groningen, The Netherlands. Email: J.G.Roelfes@rug.nl

[2] Groningen Biomolecular Sciences and Biotechnology Institute, University of Groningen, 9747 AG, Groningen, The Netherlands

Keywords: Designer enzymes, gold catalysis, thiophenol, non-canonical amino acids

One Sentence Summary: A genetically encoded thiophenol can recruit noble metals for designer enzymes catalysing abiological transformations.

Abstract:

The catalytic repertoire of nature has been expanded over the past decades by the introduction of artificial metalloenzymes. These are enzymes containing a synthetic metal complex or a non-native metal ion. However, combining noble metal catalysis and enzymes remains challenging due to the lack of suitable ligands to bind these complexes. So far, noble metal artificial metalloenzyme design mostly involves in vitro approaches of ligand anchoring, like covalent modification of a cysteine residue or via supramolecular assembly. Here, we show a facile strategy to anchor a variety of 4d- and 5d-transition metal complexes via genetic incorporation of a thiophenolic metal-binding ligand. We created a methodology to efficiently incorporate 4-mercaptophenylalanine in a protein scaffold using the stop codon suppression technology. The incorporated non-canonical amino acid was capable of binding a variety of noble metal complexes. To showcase the catalytic applications of this methodology, we developed an artificial hydroaminase by binding gold ions to the thiophenol-containing protein. The benefit of in vivo incorporation of the ligand is demonstrated by the susceptibility of catalytic activity to the microenvironment around the metal site, which can be modulated by changing the position of the ligand within the protein or by mutation of residues in its proximity.

Metalloenzymes catalyse many of the challenging chemical transformations that are essential for life with unmatched activities and selectivities.[1,2] To enable these reactions, they primarily rely on 3d-transition metals. In contrast, in synthetic chemistry, noble metal catalysis is omnipresent due to its unique and diverse reaction scope, which includes reaction classes that are not available in nature, such as cross-coupling reactions, olefin metathesis, and alkyne activation.[3–6] The desire to expand the catalytic repertoire of biocatalysis beyond the transformations known in nature has given rise to artificial metalloenzymes (ArMs), which are hybrids comprising abiological metal ions or complexes embedded in natural or designed protein scaffolds.[7] Many of these ArMs feature noble metals in the active site to bring their unique chemistry into the realm of biocatalysis. Noble metals, especially in their low oxidation states, generally require soft polarisable ligands, such as *N*-heterocyclic carbenes (NHCs) and phosphines, which are not available in nature's canon of amino acids. Hence, dative anchoring of noble metals in proteins is virtually non-existent.[8,9] Therefore, ArMs featuring noble metals are mainly constructed from pre-prepared complexes that are incorporated into proteins via supramolecular anchoring or bioconjugation (Fig. 1A).[10–20] This requires the additional chemical syntheses of complexes, is limited to distinct protein scaffolds, and often requires an in vitro ligand anchoring step that in certain cases needs an additional purification step.

Genetic code expansion strategies such as stop codon suppression (SCS) have emerged as a powerful tool to introduce non-canonical amino acids (ncAAs) into proteins.[21] Such ncAAs can be employed as metal-binding ligands, which removes the need for an in vitro ligand anchoring step.[22–24] Using SCS, 2,2-bipyridine alanine (BpyAla) and 8-hydroxyquinolin-3-yl alanine (HQAla) have been applied to create artificial metalloenzymes (Fig. 1B). However, these amino acids are better equipped to recruit 3d-transition metals for ArMs.[25–28] Genetically encoding common ligands for noble metal complexes, like NHCs or phosphines, has proven difficult to achieve due to their structure and their instability under aerobic conditions in a cellular environment. To date, there are no reports of ArMs containing genetically encoded noble metal binding ligands. There is an example where a masked phosphine ligand, a phosphine-borane adduct, was genetically incorporated.[29] However, the associated post-translational deprotection step required long reaction times, and metal-binding was only achieved with one metal complex. No catalysis was reported for this artificial metalloprotein.

In addition to NHCs[30,31] and phosphines[32], thiolates represent an important class of soft donor ligands for noble metal-binding.[33,34] In synthetic transition metal complexes, thiolates mainly exist as part of multidentate ligands in combination with phosphines or amines, or as sterically demanding thiophenolate ligands.[35,36] Homoleptic transition metal complexes using thiolates are rare as complexation is often accompanied by the formation of polymers and aggregates, leading to insoluble clusters.[37] As a result, creating well-defined catalytic centres involving donating thiophenolic ligands is challenging. However, in nature, the aliphatic thiol sidechain of the canonical amino acid cysteine is often used for the binding of transition metals in metalloproteins without forming aggregates.[38,39] Spatial separation of the thiolate ligands allows for the formation of defined 3d-transition metal complexes. To apply this for noble metals, we aimed to construct a metal-binding site using a thiophenolic ligand, which is a more polarisable residue than cysteine, and utilise it to bind softer transition metals, like the noble metals.

Here, we report a new class of artificial metalloenzymes featuring a genetically encoded thiophenol for binding noble metals and the application of this design approach by the creation of an artificial gold enzyme that shows efficient catalysis of abiological hydroamination reactions (Fig. 1C).

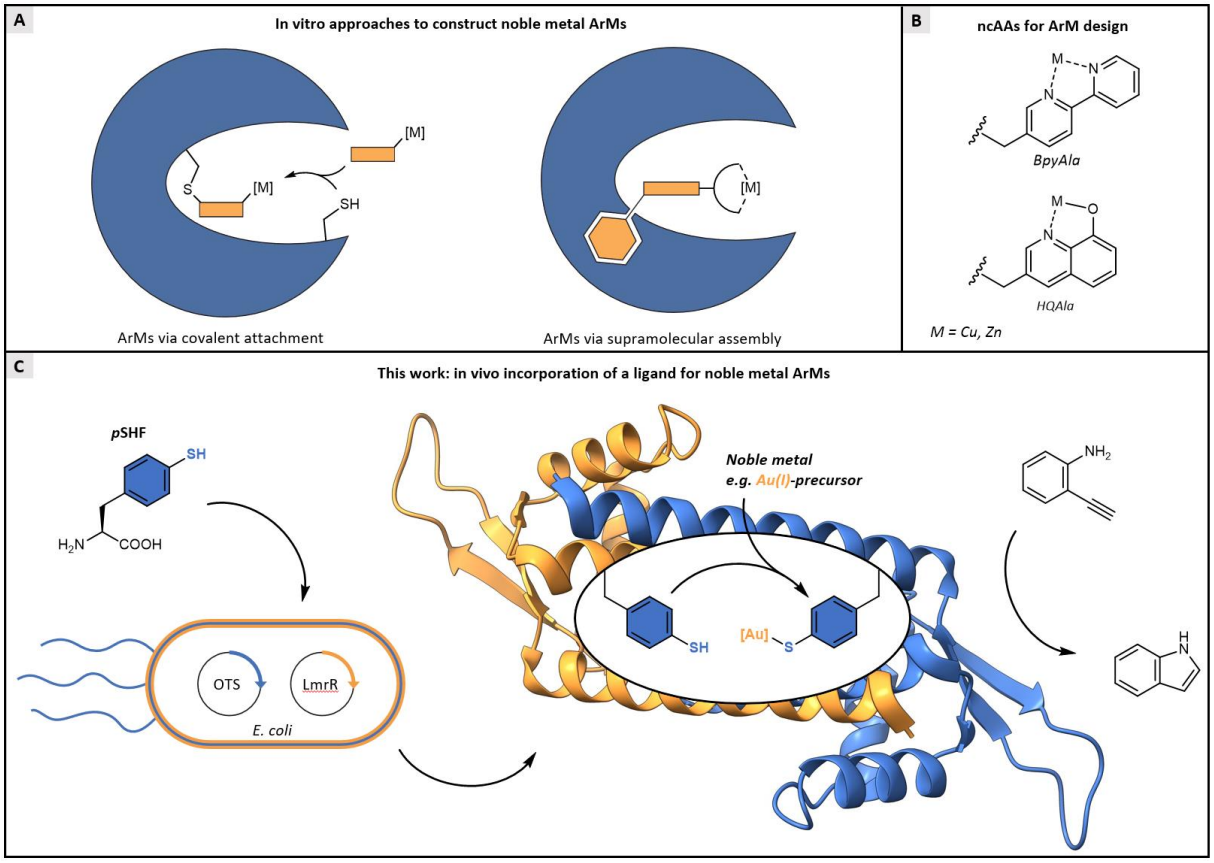

Figure 1. Context of in vivo incorporation of *p*SHF for ArM design. A. Currently most common approaches to anchor noble metal complexes to protein scaffolds for ArMs include covalent modification (left) and supramolecular assembly (right). **B.** BpyAla and HQAla expanded the metal-binding amino acid repertoire for ArM design. **C.** In vivo incorporation of a noble metal-binding ligand enables a facile strategy to synthesise noble metal ArMs (this work).

Design considerations

We selected 4-mercaptophenylalanine (*p*SHF), a thiophenolic amino acid reminiscent of tyrosine as the noble metal-binding amino acid. *p*SHF was synthesised in two steps from the commercially available *N*-Boc-4-iodo-L-phenylalanine with an overall yield of 70% (Supplementary Information section 1).[40,41] Incorporation of *p*SHF into proteins via amber stop codon suppression requires an appropriate orthogonal translation system (OTS) that consists of an aminoacyl-tRNA synthetase (aaRS) that can orthogonally load *p*SHF onto a tRNA with the anti-codon to the amber stop codon. Even though the structure of *p*SHF closely resembles the arsenal of ncAAs that have been incorporated by OTS systems based on the tyrosyl tRNA/synthetase pair of *Methanococcus jannaschii*,[21,42] no dedicated OTS has been reported for *p*SHF, to date. Therefore, we screened a library of 11 candidate OTSs to probe for promiscuous activity for the incorporation of *p*SHF, using superfolder green fluorescent protein (sfGFP) with the stop codon substitution Y151TAG (TAG = amber stop codon) as the reporter (Supplementary Information section 2).[43] From this screening, the pEVOL_pAzF OTS[44], initially developed for *para*-azido-phenylalanine (*p*AzF), was found to have promiscuous activity towards *p*SHF.

Next, we investigated the incorporation of *p*SHF into Lactococcal multidrug resistance regulator (LmrR), which has been demonstrated to be a highly versatile protein scaffold for artificial enzyme design.[45] We selected position V15 for incorporation, since this places *p*SHF inside the hydrophobic pocket at the dimer interface.[29,46] Initial attempts to incorporate *p*SHF into LmrR resulted in low protein yields (< 5 mg/L) and undesirable protein modifications. Oxidation as well as methylation of the thiol were observed in LC-MS and LC-MS/MS, respectively (Supplementary Information section 3).

The protein yield was substantially improved by switching to pEVOL_pAzF_RS.2.t1[47], which is an improved variant of the pEVOL_pAzF OTS. However, the improvement was associated with substantial misincorporation of the canonical amino acids phenylalanine and tyrosine. This problem was negated by using minimal medium with vitamins (MMV) as the expression medium, which contains lower concentrations of canonical amino acids and tRNAs during expression compared to rich media. Optimisation of the expression temperature, as well as the addition of the reductant tris(2-carboxyethyl)phosphine (TCEP) during protein production and purification, minimised modifications of the thiol group. Using the optimised protocol, after affinity chromatography purification, LmrR_V15*p*SHF was obtained in yields of 75-145 mg/L cell culture. The protocol is robust and was used for all different LmrR_*p*SHF variants. We confirmed the purity of LmrR_V15*p*SHF with HRMS and SDS-page (Supplementary Information section 4). In addition, purified LmrR_V15*p*SHF was crystallised and its structure was determined at 2.35 Å resolution, revealing well-resolved electron density for the two *p*SHF residues in the protein homodimer with no apparent chemical modifications of the thiol groups (Supplementary Information section 5).

Binding of noble metals

Having our noble metal ligand-containing protein in hand, we investigated its affinity towards noble metals. The noble metal-binding properties were assessed by electrospray ionisation mass spectrometry (ESI-MS). We conducted binding experiments by supplying a variety of noble metal ions and complexes to the apo-protein and measured adduct formation either by direct injection into the mass spectrometer or by first separating metals that are not strongly interacting with the protein using liquid chromatography (LC) (Fig. 2A, Supplementary Information section 6). LmrR_V15*p*SHF is envisioned to have two specific metal binding sites per dimer. As a control, the same experiments were performed with the LmrR protein without *p*SHF (LmrR_WT) and the corresponding cysteine variant (LmrR_V15C).

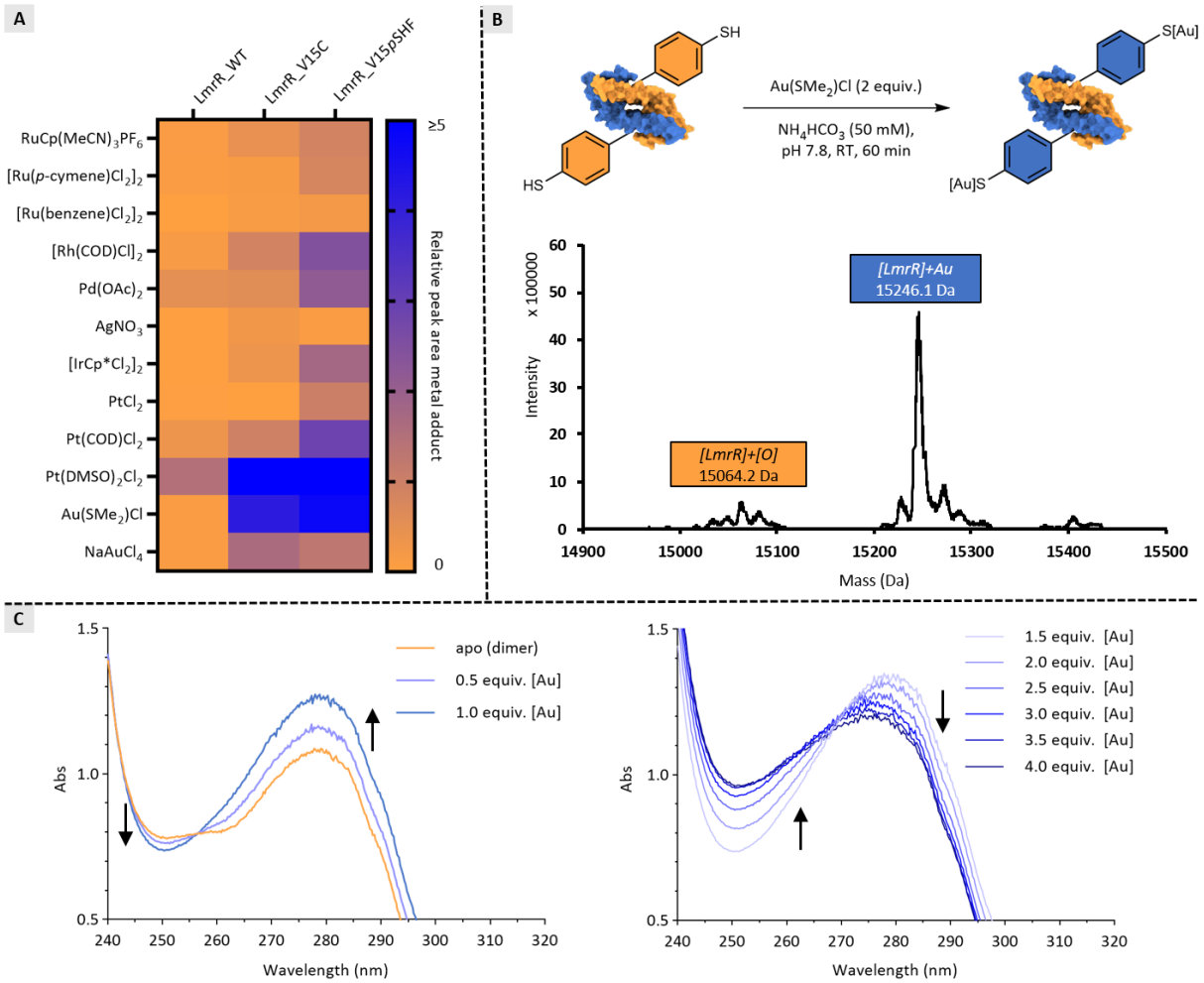

Figure 2. Evaluation of thiophenolic designer enzyme LmrR_V15*p*SHF in noble metal-binding. A. Overview of metal adduct formation of LmrR_WT, LmrR_V15C and LmrR_V15*p*SHF using LC-MS. The areas of the peaks containing LmrR with metal are divided by the areas of the peaks containing LmrR without metal. The metal precursors (2 equiv. of metal ion) were mixed with LmrR variants (1 equiv. dimer) in NH_4HCO_3 buffer. **B.** A representative example for one of the metal-binding experiments, where $Au(SMe_2)Cl$ is supplemented to LmrR_V15*p*SHF yielding LmrR_V15*p*SHF-Au. **C.** On the left, the UV-vis spectrum of 0, 0.5, and 1 equiv. of $Au(SMe_2)Cl$ titrated to LmrR_V15*p*SHF (dimer). On the right, the UV-vis spectrum of 1.5-4 equiv. of $Au(SMe_2)Cl$ titrated to LmrR_V15*p*SHF (dimer).

The artificial metalloproteins were readily formed in situ by mixing the metal precursors with the protein scaffold at ambient temperature. To our delight, LmrR_V15*p*SHF binds a variety of noble metals, albeit with varying degrees of efficiency and sometimes accompanied by oxidation. Metal complexes with ligands like cyclopentadiene (Cp), pentamethylcyclopentadiene (Cp*), or 1,5-cyclooctadiene (COD) predominantly retained that ligand after binding to the proteins. Precursors like $Au(SMe_2)Cl$ and $Pd(OAc)_2$, upon combination with the protein, showed the formation of a single species in ESI-MS, corresponding to the (LmrR_V15*p*SHF + metal) mass. In most cases, there was substantially more of the metal adduct detectable for LmrR_V15*p*SHF compared to LmrR_WT and LmrR_V15C, showing the potency of *p*SHF in binding noble metal ions or complexes. No binding was observed when using metal precursors with high oxidation states, like RuI_3, $RuCl_3$, and $RhCl_3$, which is in accordance with the Hard and Soft, Acids and Bases (HSAB) principle.[48]

Based on the rapid and clean conversion observed under MS-conditions for LmrR_V15*p*SHF with $Au(SMe_2)Cl$ (LmrR_V15*p*SHF-Au from here on) (Fig. 2B), we investigated this metalloprotein further. Since LmrR_WT does not show significant binding of $Au(SMe_2)Cl$ in LC-MS, we hypothesised that *p*SHF plays a key role in the binding. To confirm this hypothesis, $Au(SMe_2)Cl$ was titrated to LmrR_WT and

LmrR_V15*p*SHF and monitored by UV-vis spectroscopy. Indeed, no changes were observed in the UV-vis spectrum when Au(SMe_2)Cl was titrated to LmrR_WT. In contrast, titrating Au(SMe_2)Cl into LmrR_V15*p*SHF solutions resulted in notable changes in the absorption spectra (Fig. 2C). Up to a 1:1 [Au]:LmrR_V15*p*SHF (dimer) ratio, an increase of the absorption band at 280 nm, and a decrease in absorption at 250 nm with an isosbestic point at 257 nm was detected. Further addition of Au(SMe_2)Cl resulted in a distinctive change of the absorption spectra, which indicates a different interaction of the second gold ion with the protein scaffold. When gold is titrated to thiophenol, the absorption peaks disappear at higher gold concentrations, which indicates that the formation of thiophenol-Au gives rise to insoluble complexes (Supplementary Information section 7).[49,50] Aggregate formation of LmrR_V15*p*SHF-Au is avoided, because the two thiophenolic residues are spatially separated in the protein dimer. The folding of LmrR_V15*p*SHF appears to be intact upon gold-binding, since no changes in CD-spectroscopy are observed after addition of Au(SMe_2)Cl to LmrR_V15*p*SHF (Supplementary Information section 8).

After establishing the incorporation and position of the *p*SHF residues in LmrR using X-ray crystallography (Fig. 3A), we aimed to establish the binding mode of the gold ions in LmrR_V15*p*SHF. An X-ray crystal structure at 2.50 Å resolution was obtained via co-crystallisation with $KAuCN_2$, which is more water-soluble than Au(SMe_2)Cl and has been used extensively for heavy atom phasing in protein X-ray crystallography.[51] The crystal structure and crystallographic Fourier maps revealed the presence of one gold ion, coordinating one of the two *p*SHF residues in the LmrR_V15*p*SHF dimer (Fig. 3B, Supplementary Information section 9). The gold atom is associated with a strong peak in the anomalous difference Fourier map, unambiguously establishing its identity and position in the crystal structure. In addition to the sulphur of the *p*SHF residue, a hydroxyl ion or water molecule appears to serve as a coordinating ligand of the gold ion, establishing a linear two-coordination arrangement that is typical for Au(I).[52,53] The gold atom is surrounded by the side chains of Asn19, Lys22, Phe93, and Met89 at a minimal distance of 4-5 Å, establishing a second coordination sphere and restricting the solvent accessibility of the gold. No clear anomalous difference peak is present near the other *p*SHF residue, and the electron density of this residue appears distorted and weak compared to its counterpart in the dimer, indicative of substantial conformational disorder. Although it is possible that gold is also bound to this second *p*SHF residue, contributing to the observed disorder, the X-ray data is insufficient to determine this conclusively.

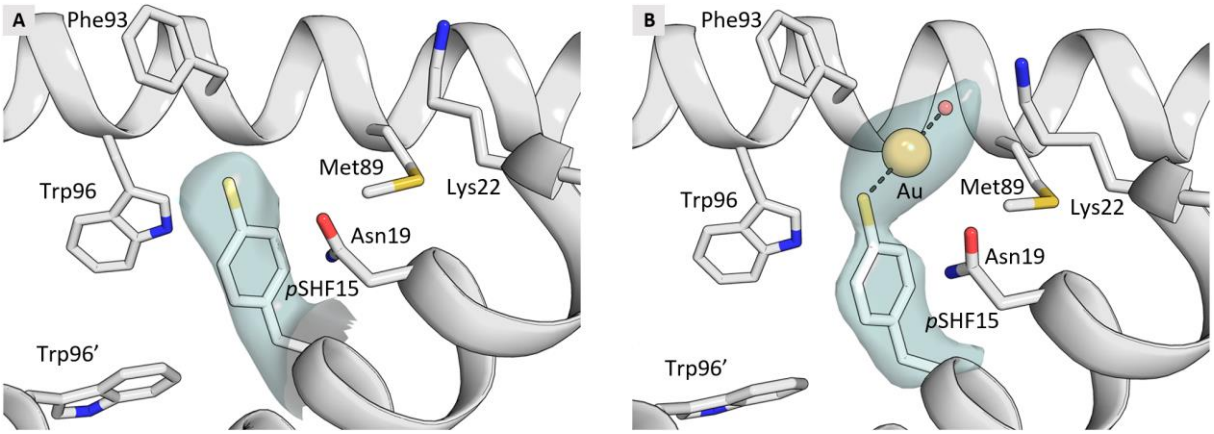

Figure 3. Crystal structures of apo and Au-bound LmrR_V15*p*SHF. A. Close-up view of apo LmrR_V15*p*SHF (PDB: 9G51), showing one of the two *p*SHF15 residues and surrounding amino acids as sticks. The cyan surface represents the Fo-Fc omit Fourier density of *p*SHF15 contoured at 2.5σ. **B.** Similar close-up view of Au-bound LmrR_V15*p*SHF (PDB: 9G52). The Fo-Fc omit Fourier density (cyan) of *p*SHF15 and the gold ion (together with a coordinating water or hydroxide ion) was contoured at 3σ.

Au-catalysed hydroamination

The thiophenolic ligand allows us to have a defined noble metal centre in the protein scaffold. To probe if the protein environment can enable catalytic activity, we evaluated LmrR_V15*p*SHF in combination with various metal precursors in an intramolecular hydroamination reaction of 2-ethynylaniline (**1**) to form indole (**2**). These reactions are catalysed by a variety of transition metal catalysts.[54–58] We probed Ru, Pt, Rh, and Au-precursors in combination with LmrR_V15*p*SHF, using a stoichiometry of one metal ion per *p*SHF (so two metal ions per dimer) as catalyst (Supplementary Information section 10). To our delight, both $Au(SMe_2)Cl$ and $NaAuCl_4$, in combination with LmrR_V15*p*SHF, exhibited substantial reactivity, while the precursors without the protein scaffold only showed trace activity. In case of Au(III)-binding, substantial oxidative damage of the protein was observed, which we hypothesised to result from Au(III) being reduced in situ to Au(I) by oxidising the protein. Therefore, we decided to continue with $Au(SMe_2)Cl$ as the metal precursor for ArM assembly. After reaction optimisation, LmrR_V15*p*SHF-Au gave rise to >50 turnover numbers (TONs) (Table 1, Supplementary Information section 11), which is comparable to artificial gold-enzymes that are constructed with NHC-ligands by supramolecular assembly.[12,14,59] At least 2-fold lower TON values were obtained using LmrR variants with cysteine, tyrosine, or other metal-binding ncAAs in the pocket (Supplementary Information section 12). The comparably low activity of the cysteine-ligated gold centre is notable. It has been shown in engineered ferritin-based systems that cysteine-ligated gold centres are active in the catalysis of intramolecular hydrolactonisation, a reaction related to the intramolecular hydroamination studied here. However, in this case the cysteine is proposed to serve as a bridging ligand between two gold centres, of which one is catalytically active.[60]

The addition of a water-soluble phosphine (TCEP) completely inactivated the catalyst. This is most likely due to the strong binding of the phosphine to the catalytic gold centre, thus making it unavailable for catalysis. Intriguingly, when using only one equivalent of gold per LmrR_V15*p*SHF dimer, no conversion was obtained, showing that a >1:1 [Au]:LmrR_V15*p*SHF (dimer) stoichiometry is necessary to obtain catalytic activity (Supplementary Information section 13).

Table 1. Intramolecular hydroamination reaction catalysed by different LmrR variants.

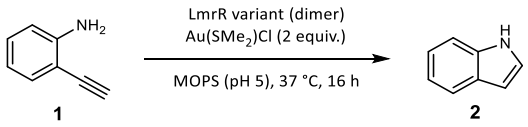

1 2

Entry	LmrR variant	Au-equivalence	TON
1	LmrR_V15*p*SHF	2 equiv. (20 μM)	56±12
2	LmrR_V15*p*SHF	1 equiv. (10 μM)	0±0
3	LmrR_V15*p*SHF	-	0±0
4	No protein	2 equiv. (20 μM)	4±0
5	LmrR_WT	2 equiv. (20 μM)	21±4
6	LmrR_V15C	2 equiv. (20 μM)	9±1
7	LmrR_V15Y	2 equiv. (20 μM)	17±3

Reaction conditions: 1 mM substrate **1**, 1 mol% ArM, 20 mM MOPS, 150 mM NaCl, pH 5, 2.6 %v/v MeCN, 37 °C, 850 rpm, 16 h
[a] Yields and conversions are obtained by GC-FID using mesitylene as internal standard.
Results are obtained as an average of two experiments, errors are given as ±(standard deviation).

To gain further insight into the relation between [Au]-stoichiometry and activity, we investigated a reaction in which urea substrate (**3**) converts either into a 6-*exo-dig* cyclisation product (**4**), through π-activation by a single gold centre, or a 5-*endo-dig* cyclisation product (**5**), through σ,π-activation by two gold centres (Fig. 4A).[14,61] Using $Au(SMe_2)Cl$ or LmrR_WT-Au gave rise to the formation of both products, with a preference for product **4**. While increasing the concentration of gold led to higher yields of **4** and **5**, the selectivity remained the same.

In contrast, no product was formed when using a 1:1 [Au]:LmrR_V15*p*SHF (dimer) ratio, similar to what was observed in the hydroamination of substrate **1**. Notably, using a 2:1 [Au]:LmrR_V15*p*SHF (dimer) ratio gave a good activity with near complete selectivity towards product **4**. Using more gold, so a ratio of >2:1 [Au]:LmrR_V15*p*SHF (dimer), an increasing amount of product **5** was observed, eventually approaching the same product ratio as obtained with LmrR_WT-Au (Fig. 4B, Supplementary Information section 14).

The fact that at a 2:1 [Au]:LmrR_V15*p*SHF (dimer) ratio almost exclusively product **4** is obtained, points to a π-activation mechanism by a single gold centre. Therefore, even though the LmrR_V15*p*SHF dimer binds two gold ions, there is no synergistic interaction between them, most likely due to spatial separation of the gold ions. Only when more $Au(SMe_2)Cl$ is added, considerable amounts of product **5** are formed. The loss of selectivity can be attributed to unspecific gold-binding or protein-free gold after the *p*SHF sites are saturated, this could then assist in the catalysis, making a σ,π-activation mechanism by two gold centres possible. Intriguing is also the absence of any catalytic activity when only one equivalent of $Au(SMe_2)Cl$ per LmrR_V15*p*SHF dimer is used, both in this reaction and in the hydroamination of substrate **1**. In agreement with the UV-vis results and the X-ray crystal structure, this suggests that the two gold binding sites are not equivalent. A hypothesis is that the first gold that is bound is inducing structural changes, i.e. causing asymmetry of the protein dimer structure, such that the second gold is the catalytic site that engages in the reaction. However, more structural evidence is needed to support this hypothesis.

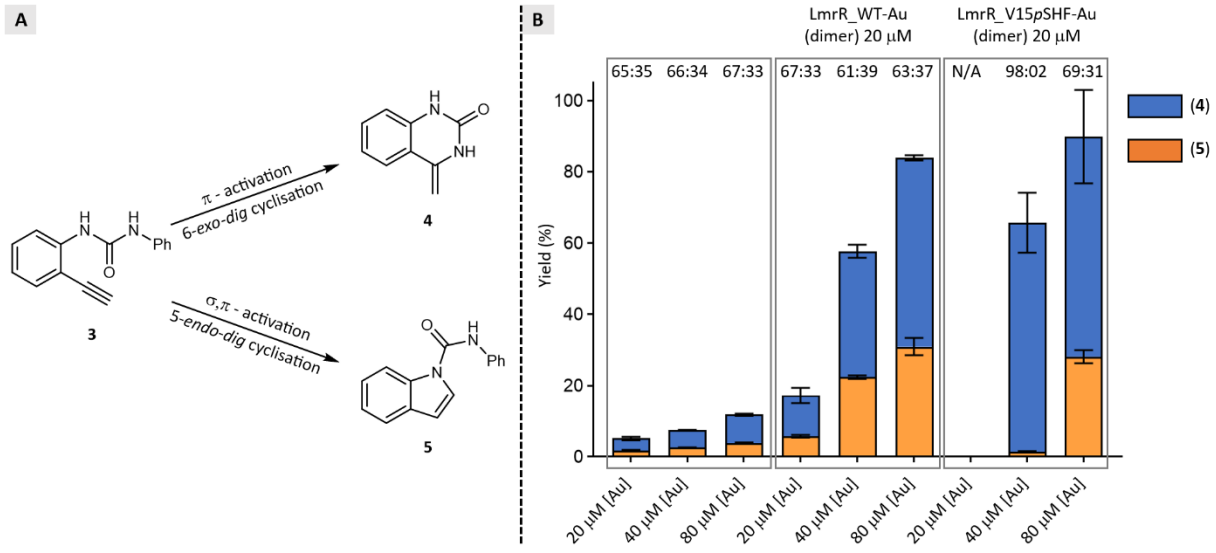

Figure 4. Gold ArM catalysed intramolecular hydroamination of substrate 3. A. Single π-activation or dual σ,π-activation of the substrate will afford a 6-*exo-dig* cyclisation product (**4**) or a 5-*endo-dig* cyclisation product (**5**), respectively. **B**. Yield and selectivity profiles with different scaffolds and varying equivalence of $Au(SMe_2)Cl$. Results are obtained as an average of two experiments, and errors are given as ±(standard deviation).

Probing the second coordination sphere

An attractive feature of the genetic incorporation of a metal-binding ligand is the close proximity of surrounding amino acids that can interact with the metal as a second coordination sphere. The effect of the environment around the gold centre was investigated by varying the position of the *p*SHF within the hydrophobic pore and mutagenesis of the residues close to the gold centre. To facilitate increased throughput methodologies for enzyme screening, we selected 2-(phenylethynyl)aniline (**6**) as a substrate. The intramolecular hydroamination of the internal alkyne gives rise to 2-phenylindole (**7**), which is fluorescent and thus allows for experiments to be performed in a plate reader (Fig. 5A, Supplementary Information section 15). In addition, the observed background reactivity was drastically reduced compared to substrate **1**, as is evident from the results of LmrR_WT-Au (Fig. 6). Using cell-free extracts for the screening of reactivity proved not feasible due to the presence of inhibiting cellular components. Therefore, we used the C-terminally fused Strep-tag II to bind the LmrR variants to Strep-Tactin resin after cell lysis. This enables facile removal of other cellular components by washing and, upon sequential addition of $Au(SMe_2)Cl$ and substrate **6**, the catalytic reaction was performed using the immobilised LmrR_*p*SHF-Au variants.

We tested eight different LmrR variants with the *p*SHF placed at various positions (Supplementary Information section 16). Of these, LmrR_A11*p*SHF and LmrR_V15*p*SHF showed notable activity. The V15*p*SHF variant was selected for further optimisation, since it showed the highest activity. Next, an alanine scanning was performed to determine which residues in the second coordination sphere have an impact on the catalytic activity (Fig. 5B). This entails substituting several residues around the *p*SHF by alanine or, if the original residue was alanine, by another amino acid. Four positions in the proximity of the *p*SHF showed significantly changed activity upon mutation (Fig. 5C, Supplementary Information section 17). Of these, we selected two positions for site-saturation mutagenesis: A11, which showed a faster reaction upon substitution to leucine, and M89, which in the crystal structure is in close proximity of the *p*SHF-bound gold centre and gave rise to lower activity when replaced with alanine.

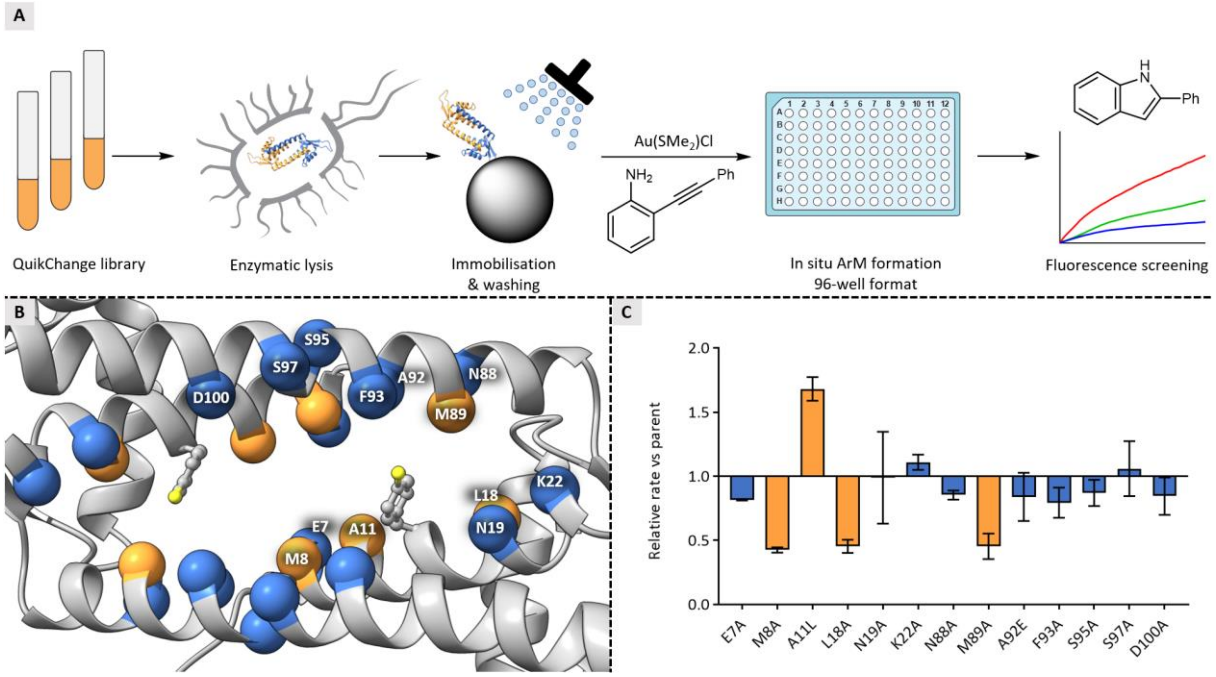

Figure 5. Mutagenesis strategy to probe the second coordination sphere of the gold centre A. Protocol to generate and screen LmrR_*p*SHF-Au variants. **B.** Various positions in and around the hydrophobic pocket were targeted for an alanine scanning. Selected positions are indicated by orange and blue spheres. For clarity, only one of the monomers is labelled. **C.** Depiction of relative rates of the alanine variants compared to the LmrR_V15*p*SHF (parent). The variants showing a significant change in reaction rate are labelled orange, whereas variants showing similar rates to the parent are labelled blue.

In case of site-saturation at position A11, improved activities were observed for several variants in the plate screen. A comparison of the isolated and purified hits confirmed the A11L variant to be the most active. Subsequently, using LmrR_V15*p*SHF_A11L as the template, position M89 was site-saturated and the variants were screened. All substitutions at this position were deleterious, which implies that the methionine at position 89 is crucial for the catalytic activity (Supplementary Information section 18).

A time course experiment on isolated and purified LmrR_V15*p*SHF_A11L-Au showed a substantial improvement in rate and yield (Fig. 6). The kinetic studies revealed a ~2.3-fold improvement in catalytic efficiency (k_{cat}/K_M) compared to LmrR_V15*p*SHF-Au (Supplementary Information section 19). Unfortunately, the improvement achieved by the A11L substitution was substrate specific, since LmrR_V15*p*SHF_A11L-Au showed a lower activity for conversion of substrate **1** compared to LmrR_V15*p*SHF-Au (Supplementary Information section 20). However, the mutagenesis studies demonstrate the evolvability of these designed scaffolds for noble metal catalysis. This is especially vital for the development of catalysts for synthetically relevant transformations that can be evolved for enantioselectivity.

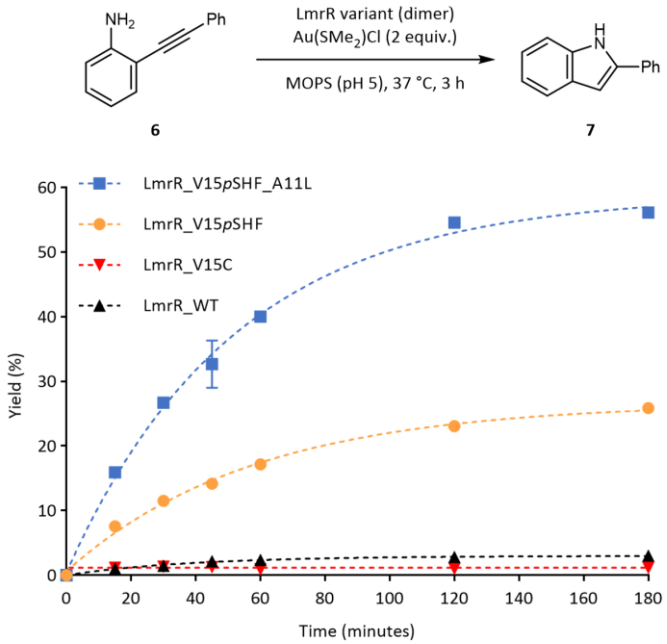

Figure 6. Time course of gold ArMs catalysing the intramolecular hydroamination of substrate 6. Relative activity of LmrR variants with indicated substitutions, displayed by yield of **7** over time. Reaction conditions: 200 μM substrate **6**, 5 μM LmrR variant, 10 μM $Au(SMe_2)Cl$, 20 mM MOPS, 150 mM NaCl, pH 5, 2.6 %v/v MeCN, 37 °C, 3 h. Results are obtained as an average of two experiments, and errors are given as ±(standard deviation).

Here we have shown that by using stop codon suppression, we can create genetically encoded noble metal-binding sites in proteins based on *p*SHF, a ncAA containing a thiophenol side chain, at any desired location. This gives convenient access to artificial noble metal enzymes for selective new-to-nature transformations, as demonstrated for the artificial gold enzyme in this study. Moreover, thiophenol ligands are under-represented in transition metal catalysis due to their propensity to form insoluble polymeric structures. As shown here, this can be circumvented by the incorporation into a protein scaffold, which keeps them in a well-defined, structurally tunable microenvironment and spatially separated from other thiophenols. Thus, this work establishes thiophenol as an attractive alternative for NHC and phosphine ligands in noble metal catalysis. Our current efforts are focused on the application of this noble metal enzyme design approach for the development of enantioselective noble metal biocatalysis of synthetically relevant reactions.

Methods

General considerations

Chemicals were purchased from Sigma-Aldrich, TCI, BLD-Pharm, Fisher scientific and Fluorochem/Doug Discovery and used without further purification. Flash column chromatography was performed using SiliaFlash P60 (40-63 μm, silicycle). ^{1}H-NMR (400 MHz) and ^{13}C-NMR (101 MHz) were recorded using a Agilent Technologies 400/54 premium shielded using DMSO-d_6 as solvent. The NMR data is reported as: chemical shift using residual solvent peaks as reference, multiplicity, coupling (Hz) and integration. *E. coli* strains XL1-blue, NEB10-β, BL21(DE3) and BL21(DE3) C43 were used for cloning and expression. *V. natriegens* (Vmax™ X2) competent cells were purchased from BioCat GmbH (Heidelberg, Germany). DENERASE® was purchased from c-LEcta GmbH (Leipzig, Germany). Primers were synthesised by Sigma-Aldrich, plasmid purification was performed using kits from QIAGEN and Phusion polymerase and Dpn1 were purchased from New England Biolabs. DNA sequencing was carried out by Eurofins Genomics. Strep-Tactin® Superflow® high capacity beads from IBA-Lifesciences were used to immobilise LmrR variants during protein purification and during library screening. Desthiobiotin from IBA-Lifesciences was used for protein purification. A Thermo Scientific Nanodrop 2000 UV-vis spectrophotometer was used to measure absorption to determine concentrations of protein (280 nm) and DNA (260 nm or 280 nm). Molar extinction coefficients at 280 nm for proteins were calculated using the ProtParam Expasy web server https://web.expasy.org/protparam/ and corrected for the presence of unnatural amino acids. Proteins were characterised via LRMS using a Waters Acquity H-class UPLC with Waters Xevo G2 QTOF or HRMS using a Thermo LTQ Orbitrap XL. Biocatalytic reactions were analysed using GC-FID (Shimadzu GC-2014) or SFC (Waters Acquity UPC2).

OTS screening

Tubes containing 5 mL LB medium with 100 μg/mL ampicillin and the respective OTS antibiotic were inoculated with *E. coli* BL21(DE3) strains containing the respective OTS plasmids and pBAD_sfGFP_Y151TAG from previously prepared glycerol stocks. The cells were incubated overnight (135 rpm, 37 °C). 50 μL of the densely grown cultures were transferred to fresh LB medium containing 100 μg/mL ampicillin and the respective OTS antibiotic. The cells were incubated (135 rpm, 37 °C) until an optical density (OD) at 600 nm of 0.3-0.6 was reached. Then, expression was induced with 5 μL 1M IPTG and 50 μL 20% L-arabinose. Meanwhile, 200 mM stock solutions of ncAAs *p*SHF and *p*AzF were prepared in DMSO. The induced cultures and the ncAAs were transferred to a 96-well plate. Each well contained 198 μL of induced *E. coli* culture expressing sfGFP-151TAG and 2 μL of 200 mM ncAA stock. *p*AzF in combination with pEVOL_pAzF served as positive control. For the negative controls no ncAA was added to the induced *E. coli* culture. The 96-well plate was placed in a fluorescence plate reader, which was preheated to 30 °C. The plate was shaken continuously, while fluorescence intensity ($\lambda_{excitation}$ = 485 nm and $\lambda_{emission}$ = 528 nm) was measured for 16 h.

Expression & purification of LmrR variants

A tube containing 5 mL LB medium (100 μg/mL ampicillin and 34 μg/mL chloramphenicol) was inoculated with a toothpick from an *E. coli* BL21(DE3) glycerol stock harbouring the plasmids pET17b_LmrR_V15TAG and pEVOL_pAzFRS.2.t1. The cells were incubated overnight (200 rpm, 37 °C). The 5 mL culture was then used to inoculate a flask containing 250 mL MMV medium (100 μg/mL ampicillin and 34 μg/mL chloramphenicol). Then, the cells were incubated (200 rpm, 37 °C) until an OD at 600 nm of 0.6-0.7 was reached. Meanwhile, a 200 mM *p*SHF + 200 mM TCEP·HCl solution in MeOH:water (1:1) with a final volume of 2.5 mL was prepared. The solution was neutralised with 10 M NaOH and incubated for 15 min at room temperature. At this point, the OTS was induced by the addition of L-arabinose (500 mg, 0.2 w/v %), and TCEP (1.25 mL of 200 mM TCEP in milliQ water pH 8, 1 mM) and the *p*SHF solution (2.5 mL, 2 mM *p*SHF) were added. The cells were incubated for 30-60 min (200 rpm, 37 °C). Then the expression of LmrR was induced with IPTG (250 μL of 1 M IPTG in milliQ water, 1 mM). The cells were incubated for 22 h (200 rpm, 24 °C). The cells were harvested by centrifugation (3000 g, 15 min, 4 °C). The supernatant was decanted, and the cell pellets were frozen at -20 °C. The next day, the cells were resuspended in washing buffer (20 mL, 50 mM NaH_2PO_4, 150 mM NaCl, pH 8.0) containing 1 mM TCEP and 1 mM EDTA. The cells were lysed by sonication (70%, 10 sec on/15 sec off, 8 min), while the tube containing the cells was placed in ice-water to cool. The lysed cells were spun down by centrifugation (18500 g, 30 min, 4 °C) and loaded onto a Strep-Tactin resin. After collecting the flow-through, it was reapplied to the Strep-Tactin resin. Then the column was washed with 4 column volumes of washing buffer + 1 mM TCEP. The protein was eluted with elution buffer (washing buffer + 5 mM desthiobiotin, 1 mM TCEP) and the fractions were collected. The fractions were combined and concentrated using a 10,000 MWCO concentrator. The purity and molecular weight of the protein were assessed by ESI-HRMS. Before use in catalysis, the protein was desalted into the reaction buffer using a Sephadex G-25 size-exclusion column. The protein concentration was determined by using the calculated extinction coefficient for LmrR, corrected for the absorbance of *p*SHF ($\varepsilon_{280,\ pH\ 5}$ = 1265 $M^{-1}\ cm^{-1}$).

Mass-spectrometry assay of metal-binding

The respective protein solutions (20 μM) were prepared in 50 mM NH_4HCO_3 (pH 7.8) and incubated with the respective metal complex (40 μM of metal) with 0-2 %v/v MeCN at room temperature. After 30-60 min and 180-240 min of incubation the samples were injected into a WatersTM Xevo G2 QTOF via a bypass column with a constant flow of 90:10 water:MeCN with 0.1 %v/v formic acid at a rate of 0.3 mL/min. After 60-180 min the samples were characterised by LC/HRMS using a WatersTM Acquity Ultra Performance LC coupled to a WatersTM Xevo G2 QTOF. The samples were injected on a ACQUITY UPLC BEH300 C4 1.7 μm column using water and MeCN with 0.1 %v/v formic acid as mobile phase with a flow rate of 0.3 mL/min. The TIC peak in the obtained chromatogram peak was extracted to get the m/z spectrum. This was deconvoluted in MagTran using a mass range of 10,000-80,000, a charge range of 1-80, a S/N threshold of 10 and a max no. of species of 10. Only if the apo protein peak was not visible under these parameters, the S/N threshold was lowered to 5. The centroid of the peaks was determined by using the Gaussian deconvolution function of MagTran on the peak of interest. The resulting mass domain was integrated in specific ranges by taking into account the calculated masses of the respective proteins and metal complexes. The peak areas containing [protein+metal] were divided by the peak areas containing protein without metal to obtain a ratio that is representative of the extent of metal adduct formation under MS conditions.

UV-vis [Au]-titration

UV-vis spectra were recorded on a SPECORD 210 PLUS spectrophotometer at room temperature in a 1 cm pathlength quartz cuvette. Samples with 20 μM LmrR variant or 40 μM thiophenol (3.33 μL, 6 mM stock in MeCN) were prepared in MOPS buffer (20 mM MOPS, 150 mM NaCl, pH 5) with a total volume of 500 μL. To this was titrated $Au(SMe_2)Cl$ in MeCN (8 x 1.25 μL, 4 mM stock, 10 μM increments). Addition of each aliquot was followed by incubation for 1-2 min at room temperature before recording the UV-vis spectrum (scan range 200-800 nm, 20 nm/s). Absorbances were corrected for dilution.

Catalysis (substrate 1)

A microcentrifuge tube (1.5 mL) was charged with freshly desalted protein (10 μM final dimer concentration) in MOPS buffer (20 mM MOPS, 150 mM NaCl, pH 5). Then a freshly prepared stock of $Au(SMe_2)Cl$ in MeCN (1.33 μL, 2.25 mM stock, 20 μM final concentration) was added to the solution. After 5 min of incubation at room temperature, substrate **1** in MeCN (2.5 μL, 60 mM stock, 1 mM final concentration) was added. The reaction mixture was shaken for 16 h (850 rpm, 37 °C). To the reaction mixture, 300 μL DCM with 250 μM mesitylene as internal standard was added. The sample was vortexed for 1 min and inverted (x3). The layers were separated by centrifugation (13000 g, 2 min). 250 μL of the organic layer was pipetted into a GC-vial and analysed by GC-FID.

Catalysis (substrate 3)

A microcentrifuge tube (1.5 mL) was charged with freshly desalted protein (10 μM final dimer concentration) in MOPS buffer (20 mM MOPS, 150 mM NaCl, pH 5). Then a freshly prepared stock of $Au(SMe_2)Cl$ in MeCN (varying concentrations depending on [Au] equiv.) was added to the solution. MeCN was added appropriately to get a final concentration of 3.3 %v/v MeCN. After 5 min of incubation at room temperature, substrate **3** in MeCN (2.5 μL, 60 mM stock, 1 mM final concentration) was added. The reaction mixture was shaken for 16 h (850 rpm, 37 °C). The tube was centrifuged (13000 g, 30 sec) and 300 μL DCM with 250 μM 2-phenylquinoline as internal standard was added. The sample was vortexed (1 min) and inverted (x3). The layers were separated by centrifugation (13000 g, 2 min). 290 μL of the organic layer was pipetted into a new microcentrifuge tube (1.5 mL) and the solvent was removed in vacuo (15 min, 30 °C). The residue was redissolved in SFC grade MeOH (80 μL) and analysed by SFC.

Library preparation & screening

5 mL main cultures of the targeted mutants were grown as described in the expression protocol. The cells were transferred to a 15 mL tube and harvested by centrifugation (3000 g, 15 min). The supernatant was decanted and the cell-pellets were frozen overnight at -20 °C. The cell-pellets were resuspended in 500 μL lysis buffer (20 mM MOPS, 150 mM NaCl, 1 mg/mL lysozyme (from chicken egg white), 0.1 mg/mL DNaseI, 10 mM $MgSO_4$). The OD at 600 nm was measured (1:10 dilution with milliQ water). The tubes were incubated for 2 h (200 rpm, 30 °C). The lysed cells were transferred to 1.5 mL microcentrifuge tubes and spun-down (17000 g, 5 min). The OD-normalised lysates (lowest OD = 140 μL) were mixed with bead solution (200 μL for A11X-library or 100 μL for M89X-library of Strep-Tactin® Superflow® high capacity, 50 % suspension). 600 μL of phosphate buffer (50 mM NaH_2PO_4, 150 mM NaCl, pH 8.0) was added and the mixture was vortexed (1 min), incubated for 4 min at room temperature and centrifuged (17000 g, 2 min). The supernatant was discarded and the beads were resuspended in 600 μL MOPS buffer (20 mM MOPS, 150 mM NaCl, pH 7) and centrifuged (17000 g, 2 min). The supernatant was discarded and the beads were resuspended in 600 μL MOPS buffer (20 mM MOPS, 150 mM NaCl, pH 5) and centrifuged (17000 g, 2 min). The supernatant was fully discarded and the beads were resuspended in 200 μL for A11X-library or 300 μL for M89X-library MOPS buffer (20 mM MOPS, 150 mM NaCl, pH 5). The bead solutions (140 μL per well, duplicates) were added to a 96-well microplate (Nunc™ F96 MicroWell™, black, polystyrene, ThermoFisher). Then, a freshly prepared stock of $Au(SMe_2)Cl$ in MeCN (5 μL, 300 μM stock, 10 μM final concentration) was added to each well and incubated for 5 min at room temperature. Finally, a freshly prepared stock of substrate **6** in MeCN (5 μL, 30 mM stock, 1 mM final concentration) was added to each well. Kinetic measurements were performed in a microplate reader (Synergy H1, BioTek) at 37 °C with double orbital shaking by measuring relative fluorescence intensity ($\lambda_{excitation}$= 320 nm and $\lambda_{emission}$ = 365 nm).

Kinetics & time course

A microcentrifuge tube (1.5 mL) was charged with a mixture of 5 μM freshly desalted LmrR variant, 10 μM $Au(SMe_2)Cl$ and MeCN (final concentration 10 %v/v) in MOPS buffer (20 mM MOPS, 150 mM NaCl, pH 5). After 5 min of incubation at room temperature, substrate **6** in MeCN (varying concentrations, for time course: 200 μM final concentration) was added to reach a total volume of 150 μL. The reaction mixture was incubated for 30 min (850 rpm, 37 °C) (for time course: varying incubation times). Then the tube was put on ice and was quenched with TCEP (0.6 μL, 50 mM stock in phosphate buffer pH 8, 200 μM final concentration). The tube was centrifuged (13000 g, 30 sec), 300 μL DCM with 50 μM 2-phenylquinoline as internal standard was added. The sample was vortexed (1 min) and inverted (x3). The layers were separated by centrifugation (13000 g, 2 min). 290 μL of the organic layer was pipetted into a new microcentrifuge tube (1.5 mL) and the solvent was removed in vacuo (15 min, 30 °C). The residue was redissolved in SFC grade MeOH (80 μL) and analysed by SFC.

References

1. Torres, E. & Ayala, M. Biocatalysis by Metalloenzymes. in *Comprehensive Inorganic Chemistry II* 685–735 (Elsevier, 2013). doi:10.1016/B978-0-08-097774-4.00625-2.
2. Andreini, C., Bertini, I., Cavallaro, G., Holliday, G. L. & Thornton, J. M. Metal ions in biological catalysis: from enzyme databases to general principles. *J. Biol. Inorg. Chem.* **13**, 1205–1218 (2008).
3. Suzuki, A. Cross-Coupling Reactions Of Organoboranes: An Easy Way To Construct C-C Bonds (Nobel Lecture). *Angew. Chem. Int. Ed.* **50**, 6722–6737 (2011).
4. Ogba, O. M., Warner, N. C., O'Leary, D. J. & Grubbs, R. H. Recent advances in ruthenium-based olefin metathesis. *Chem. Soc. Rev.* **47**, 4510–4544 (2018).
5. Fürstner, A. & Davies, P. W. Catalytic Carbophilic Activation: Catalysis by Platinum and Gold π Acids. *Angew. Chem. Int. Ed.* **46**, 3410–3449 (2007).
6. Hashmi, A. S. K. & Hutchings, G. J. Gold Catalysis. *Angew. Chem. Int. Ed.* **45**, 7896–7936 (2006).
7. Schwizer, F. *et al.* Artificial Metalloenzymes: Reaction Scope and Optimization Strategies. *Chem. Rev.* **118**, 142–231 (2018).
8. Key, H. M., Clark, D. S. & Hartwig, J. F. Generation, Characterization, and Tunable Reactivity of Organometallic Fragments Bound to a Protein Ligand. *J. Am. Chem. Soc.* **137**, 8261–8268 (2015).
9. Jing, Q., Okrasa, K. & Kazlauskas, R. J. Stereoselective Hydrogenation of Olefins Using Rhodium-Substituted Carbonic Anhydrase—A New Reductase. *Chem. Eur. J.* **15**, 1370–1376 (2009).
10. Laureanti, J. A. *et al.* Protein Scaffold Activates Catalytic CO2 Hydrogenation by a Rhodium Bis(diphosphine) Complex. *ACS Catal.* **9**, 620–625 (2019).
11. Skander, M. *et al.* Artificial Metalloenzymes: (Strept)avidin as Host for Enantioselective Hydrogenation by Achiral Biotinylated Rhodium−Diphosphine Complexes. *J. Am. Chem. Soc.* **126**, 14411–14418 (2004).

12. Chang, T.-C., Vong, K., Yamamoto, T. & Tanaka, K. Prodrug Activation by Gold Artificial Metalloenzyme-Catalyzed Synthesis of Phenanthridinium Derivatives via Hydroamination. *Angew. Chem. Int. Ed.* **133**, 12554–12562 (2021).
13. Yang, H., Srivastava, P., Zhang, C. & Lewis, J. C. A General Method for Artificial Metalloenzyme Formation through Strain-Promoted Azide–Alkyne Cycloaddition. *ChemBioChem* **15**, 223–227 (2014).
14. Christoffel, F. *et al.* Design and evolution of chimeric streptavidin for protein-enabled dual gold catalysis. *Nat. Catal.* **4**, 643–653 (2021).
15. Vornholt, T. *et al.* Systematic engineering of artificial metalloenzymes for new-to-nature reactions. *Sci. Adv.* **7**, eabe4208 (2021).
16. Kato, S., Onoda, A., Schwaneberg, U. & Hayashi, T. Evolutionary Engineering of a Cp*Rh(III) Complex-Linked Artificial Metalloenzyme with a Chimeric β-Barrel Protein Scaffold. *J. Am. Chem. Soc.* **145**, 8285–8290 (2023).
17. Yang, H. *et al.* Evolving artificial metalloenzymes via random mutagenesis. *Nat. Chem.* **10**, 318–324 (2018).
18. Key, H. M., Dydio, P., Clark, D. S. & Hartwig, J. F. Abiological catalysis by artificial haem proteins containing noble metals in place of iron. *Nature* **534**, 534–537 (2016).
19. Hyster, T. K., Knörr, L., Ward, T. R. & Rovis, T. Biotinylated Rh(III) Complexes in Engineered Streptavidin for Accelerated Asymmetric C–H Activation. *Science* **338**, 500–503 (2012).
20. Jeschek, M. *et al.* Directed evolution of artificial metalloenzymes for in vivo metathesis. *Nature* **537**, 661–665 (2016).
21. Wang, L., Brock, A., Herberich, B. & Schultz, P. G. Expanding the Genetic Code of Escherichia coli. *Science* **292**, 498–500 (2001).
22. Xie, J., Liu, W. & Schultz, P. G. A Genetically Encoded Bidentate, Metal-Binding Amino Acid. *Angew. Chem. Int. Ed.* **119**, 9399–9402 (2007).

23. Lee, H. S., Spraggon, G., Schultz, P. G. & Wang, F. Genetic incorporation of a metal-ion chelating amino acid into proteins as a biophysical probe. *J. Am. Chem. Soc.* **131**, 2481–2483 (2009).
24. Hu, C., I. Chan, S., B. Sawyer, E., Yu, Y. & Wang, J. Metalloprotein design using genetic code expansion. *Chem. Soc. Rev.* **43**, 6498–6510 (2014).
25. Drienovská, I., Rioz-Martínez, A., Draksharapu, A. & Roelfes, G. Novel artificial metalloenzymes by in vivo incorporation of metal-binding unnatural amino acids. *Chem. Sci.* **6**, 770–776 (2015).
26. Drienovská, I., Scheele, R. A., Gutiérrez de Souza, C. & Roelfes, G. A Hydroxyquinoline-Based Unnatural Amino Acid for the Design of Novel Artificial Metalloenzymes. *ChemBioChem* **21**, 3077–3081 (2020).
27. Klemencic, E., C. Brewster, R., S. Ali, H., M. Richardson, J. & G. Jarvis, A. Using BpyAla to generate copper artificial metalloenzymes: a catalytic and structural study. *Catal. Sci. Technol.* **14**, 1622–1632 (2024).
28. Yang, M. & Song, W. J. Diverse protein assembly driven by metal and chelating amino acids with selectivity and tunability. *Nat. Commun.* **10**, 5545 (2019).
29. Duan, H.-Z. *et al.* Genetically Encoded Phosphine Ligand for Metalloprotein Design. *J. Am. Chem. Soc.* **144**, 22831–22837 (2022).
30. Zhao, Q., Meng, G., Nolan, S. P. & Szostak, M. N-Heterocyclic Carbene Complexes in C–H Activation Reactions. *Chem. Rev.* **120**, 1981–2048 (2020).
31. Nolan, S. P. *N-Heterocyclic Carbenes: Effective Tools for Organometallic Synthesis*. (Wiley, 2014).
32. van Leeuwen, P. W. N. M. & Kamer, P. C. J. *Phosphorus(III)Ligands in Homogeneous Catalysis: Design and Synthesis*. (Wiley, 2012).
33. Yoshinari, N., Kuwamura, N., Kojima, T. & Konno, T. Development of coordination chemistry with thiol-containing amino acids. *Coord. Chem. Rev.* **474**, 214857 (2023).
34. Pearson, R. G. & Songstad, J. Application of the Principle of Hard and Soft Acids and Bases to Organic Chemistry. *J. Am. Chem. Soc.* **89**, 1827–1836 (1967).

35. Marco H. Klingele, J. K. & Kersting, B. The Chemistry of Metal Thiophenolates. in *PATAI's Chemistry of Functional Groups* (Wiley & Sons, 2013). doi:10.1002/9780470682531.pat0608.
36. Chuchuryukin, A. V. *et al.* Hydroxy- and Mercaptopyridine Pincer Platinum and Palladium Complexes Generated by Silver-Free Halide Abstraction. *Inorg. Chem.* **45**, 2045–2054 (2006).
37. Taut, J., Chambron, J.-C. & Kersting, B. Fifty Years of Inorganic Biomimetic Chemistry: From the Complexation of Single Metal Cations to Polynuclear Metal Complexes by Multidentate Thiolate Ligands. *Eur. J. Inorg. Chem.* **26**, e202200739 (2023).
38. Pace, N. J. & Weerapana, E. Diverse Functional Roles of Reactive Cysteines. *ACS Chem. Biol.* **8**, 283–296 (2013).
39. Giles, N. M. *et al.* Metal and Redox Modulation of Cysteine Protein Function. *Chem. Biol.* **10**, 677–693 (2003).
40. Rajagopalan, S., Radke, G., Evans, M. & Tomich, J. M. Synthesis of N-t-Boc-4-S-t-Butyl-L-thiophenylalanine via Palladium Catalyzed Cross-Coupling Reaction of N-t-Boc-4-Iodo-L-phenylalanine with t-Butylthiol or Sodium t-Butylthiolate. *Synth. Commun.* **26**, 1431–1440 (1996).
41. Rudolf, J. D. & Poulter, C. D. Tyrosine O-Prenyltransferase SirD Catalyzes S-, C-, and N-Prenylations on Tyrosine and Tryptophan Derivatives. *ACS Chem. Biol.* **8**, 2707–2714 (2013).
42. Dumas, A., Lercher, L., D. Spicer, C. & G. Davis, B. Designing logical codon reassignment – Expanding the chemistry in biology. *Chem. Sci.* **6**, 50–69 (2015).
43. Rubini, R., Ivanov, I. & Mayer, C. A Screening Platform to Identify and Tailor Biocompatible Small-Molecule Catalysts. *Chem. Eur. J.* **25**, 16017–16021 (2019).
44. Chin, J. W. *et al.* Addition of p-Azido-l-phenylalanine to the Genetic Code of Escherichia coli. *J. Am. Chem. Soc.* **124**, 9026–9027 (2002).
45. Roelfes, G. LmrR: A Privileged Scaffold for Artificial Metalloenzymes. *Acc. Chem. Res.* **52**, 545–556 (2019).

46. Drienovská, I., Mayer, C., Dulson, C. & Roelfes, G. A designer enzyme for hydrazone and oxime formation featuring an unnatural catalytic aniline residue. *Nat. Chem.* **10**, 946–952 (2018).
47. Amiram, M. *et al.* Evolution of translation machinery in recoded bacteria enables multi-site incorporation of nonstandard amino acids. *Nat. Biotechnol.* **33**, 1272–1279 (2015).
48. Pearson, R. G. Hard and Soft Acids and Bases. *J. Am. Chem. Soc.* **85**, 3533–3539 (1963).
49. Dyadchenko, V. P. *et al.* A complex of gold(I) benzenethiolate with isocyanide: synthesis and crystal and molecular structures. *Russ. Chem. Bull. Int. Ed.* **59**, 539–543 (2010).
50. Schmidbaur, H. & Schier, A. Aurophilic interactions as a subject of current research: an up-date. *Chem. Soc. Rev.* **41**, 370–412 (2012).
51. Garman, E. & Murray, J. W. Heavy-atom derivatization. *Acta Crystallogr. D* **59**, 1903–1913 (2003).
52. Forward, J. M., Bohmann, D., Fackler, J. P. Jr. & Staples, R. J. Luminescence Studies of Gold(I) Thiolate Complexes. *Inorg. Chem.* **34**, 6330–6336 (1995).
53. Hao, L., Mansour, M. A., Lachicotte, R. J., Gysling, H. J. & Eisenberg, R. A Gold(I) Mononuclear Complex and Its Association into Binuclear and Cluster Compounds by Hydrogen Bonding or Metal Ion Coordination. *Inorg. Chem.* **39**, 5520–5529 (2000).
54. Wang, H. *et al.* Ruthenium(II)-Catalyzed Hydroamination of Allenoates: A Regioselective Synthesis of Allylamines. *Adv. Synth. Catal.* **364**, 4152–4156 (2022).
55. Chen, Q.-A., Chen, Z. & Dong, V. M. Rhodium-Catalyzed Enantioselective Hydroamination of Alkynes with Indolines. *J. Am. Chem. Soc.* **137**, 8392–8395 (2015).
56. Brunet, J.-J., Chu, N. C., Diallo, O. & Vincendeau, S. Platinum-catalyzed intermolecular hydroamination of terminal alkynes. *J. Mol. Catal. Chem.* **240**, 245–248 (2005).
57. Widenhoefer, R. A. & Han, X. Gold-Catalyzed Hydroamination of C–C Multiple Bonds. *Eur. J. Org. Chem.* **2006**, 4555–4563 (2006).
58. Tashrifi, Z., Mohammadi Khanaposhtani, M., Biglar, M., Larijani, B. & Mahdavi, M. Recent Advances in Alkyne Hydroamination as a Powerful Tool for the Construction of C–N Bonds. *Asian J. Org. Chem.* **9**, 969–991 (2020).

59. Ebensperger, P. *et al.* A Dual-Metal-Catalyzed Sequential Cascade Reaction in an Engineered Protein Cage. *Angew. Chem. Int. Ed.* **62**, e202218413 (2023).

60. Lu, C. *et al.* Novel Au(I)-Based Artificial Metallo-Cycloisomerase for Catalyzing the Cycloisomerization of γ-Alkynoic Acids. *ACS Catal.* **13**, 9918–9924 (2023).

61. Gimeno, A. *et al.* Competitive Gold-Activation Modes in Terminal Alkynes: An Experimental and Mechanistic Study. *Chem. Eur. J.* **20**, 683–688 (2014).

Acknowledgements

We thank J.L. Sneep, J. Hekelaar and F.Y. Ho for analytical support. We thank W.R. Browne for providing spectroscopy equipment. This work was supported by the European Research Council (ERC advanced grant 885396). We acknowledge the European Synchrotron Radiation Facility (ESRF) for provision of synchrotron radiation facilities and thank the scientists at beamline MASSIF-1 for their support.

Author contributions

G.R., D.F.S. and M.J.V. conceived the project. M.J.V. and F.S.A. developed and optimised the expression of LmrR_*p*SHF. M.J.V. and D.F.S. developed the hydroamination reaction. F.S.A and H.J.R. performed crystal-growing experiments. M.J.V. performed the all other experimental work for the project and wrote the original draft. A.-M.W.H.T. analysed the X-ray data. G.R. and D.F.S. directed the project. M.J.V., F.S.A., A.-M.W.H.T., D.F.S. and G.R. reviewed and edited the manuscript.

Competing interests

The authors declare no competing interests.